Thermal conductivity of argon–SiO$_2$ cryocrystal nanocomposite

R.V. Nikonkov, P. Stachowiak, and A. Jeżowski

Institute for Low Temperature and Structure Research, Polish Academy of Sciences, PN 1410, 50-950 Wroclaw, Poland
E-mail: P.Stachowiak@int.pan.wroc.pl

A.I. Krivchikov

B. Verkin Institute for Low Temperature Physics and Engineering of NAS Ukraine
47 Prospekt Nauky, Kharkiv 61103, Ukraine

The effective thermal conductivity of samples of cryocrystal nanocomposite obtained from argon and SiO$_2$ nanopowder was determined in the temperature interval 2–35 K using the steady-state method. The thermal conductivity of crystalline argon with nanoparticles of amorphous silica oxide embedded in its structure shows a weak dependence on particle linear dimension in the interval 5–42 nm. The temperature dependence of the thermal conductivity of the nanocomposites can be well approximated by taking into account only the two mechanisms of heat carrier scattering: phonon-phonon interaction in U-processes and scattering of phonons by dislocations.

Introduction

Not very long ago a new chapter in technology has been crack opened. It seems that the bulk materials using nano- and microparticles due to their particular thermal properties are going to play an important role in many future applications [1–4]. Along with the advent of the new materials, new basic problems and questions regarding the thermal transport mechanisms in bulk solids containing numerous nanoparticles in their crystalline matrices have emerged. Many thermal conduction mechanisms of the new materials were negligible or just absent from the classical ones. Therefore, the analysis of phonon transfer in crystals containing nanoparticles requires a new approach. For example, when we consider a phonon of a wave vector q, which encounters on its pathway a nanoparticle of linear dimensions R, it gets scattered. The result of the scattering depends on the so called size parameter χ, which is defined as $\chi = |\mathbf{q}| R$. When the size parameter is small ($\chi \ll 1$), the scattering rule obeys Rayleigh law, i.e., the scattering probability varies as frequency to the fourth power. At the other limit, where the size parameter reaches big numbers ($\chi \gg 1$) the scattering probability is inde-

pendent of frequency of the phonon and the phonon scattering cross section depends on the path length through which the phonon travels across the nanoparticle and the associated phase lag [5]. Thus, the size of the nanoparticle becomes a very important factor for scattering cross section in this regime. In the Rayleigh scattering regime, the scattering cross section depends both on the difference of masses of the nanoparticle and the host crystal and on the difference of the force constancies acting in the two constituencies [5]. In the case of polydispersion of nanoparticles, when the size of nanoparticles deviates from its mean value, the scattering cross section based on mean diameter increases with increasing standard deviation of the linear dimension of the nanoparticles [5]. The considerations sketched above do not exhaust the complexity of problems related to the thermal energy transfer in the discussed nanostructured objects. They can be helpful for the analysis of thermal transport processes in case of the nanoparticles being far from each other. The term "far from each other" is considered here with respect to the wavelength of the phonons. Therefore, if the ratio of distance between the nanoparticles and the wavelength is much large than 1,

then independent phonon scattering (the scattering by one nanoparticle without reference to the others) is a good approach. However, if the ratio σ of the interparticle distance d and the phonon wavelength $2\pi/|\mathbf{q}|$ is close to 1, for correct description of the thermal processes multiple and dependent phonon scatterings have to be taken into account. Here the multiple phonon scattering means that a scattered wave from one nanoparticle is incident on another particle to be scattered again while the dependent scattering is far-field interference of waves scattered by the different nanoparticles due to phase difference, which is ignored in the independent scattering regime. When $\sigma \approx 1$, the multiple elastic scattering due to nanoparticles modifies the original crystalline matrix phonons velocity, density of states and their equilibrium intensity while the dependent scattering results in change of original cross section for phonon scattering by the nanoparticles. In this indirect way the multiple and dependent processes influence the crystal thermal conductivity [6]. In a real crystal — with nanoparticles embedded in its structure — the abovementioned condition $\sigma \approx 1$ may be fulfilled when the volume density of the nanoparticles is either high enough or at low temperatures. As for the former, for a given volume fraction, the interparticle distance is smaller for smaller linear dimensions of the nanoparticles.

The effect of nanoparticles on the thermal conductivity of nanocomposites was quantitatively confirmed by numerous experiments [7–10]. Here we report our preliminary results of investigations of thermal conductivity of argon crystals containing in their volume silica nanoparticles of different linear dimensions. We have chosen the crystal because of its simplicity, both in terms of the crystallographic structure and interatomic interactions. As with other rare gas solids, it is bound by van der Waals forces and has an fcc structure in the whole range of temperatures and pressures.

The argon crystal is also the best experimentally known noble gas one. The first measurements of its thermal conductivity were made in the 1950's by White and Woods [11]. Up to now, a number of measurements have been made by other experimentators, both at constant volume and at equilibrium vapor pressure, in various temperature intervals, see e.g. [12–14].

Experiment

In our experiment the thermal conductivity of cryocrystal nanocomposites was determined by steady-state heat flow method in the temperature range from 2.2 to 35 K. The methodology of the measurement and its technical aspect have been described in details in our previous paper [15].

The thermal conductivity cell was made from glass tube of an inner diameter of 6 mm, a wall thickness of 1 mm and a length of 50 mm. To the ends of the tube two caps made of copper were fixed with epoxy. The cell was equipped with two germanium resistance thermometers spaced 10 mm from each other. The lower one was mounted 10 mm above the bottom of the ampoule. To the top cap an electric gradient heater was attached. Through the cap a thin-wall stainless steel capillary ran. The capillary allowed to pump out the cell or fill it with argon gas and thermal exchange gas of helium. During the experiment the bottom cap rested in a copper base of controlled temperature.

For obtaining the nanocomposite samples, argon gas of 99.999% purity produced by Messer Group GmbH and amorphous silica oxide nanoparticles of linear dimension of about 5 nm, 15 nm and 42 nm were used. The SiO_2 5 and 42 nm nanoparticle powders were synthesized in the Institute for Low Temperatures and Structure Research PAS, Wrocław, Poland by combustion method while the one of 15 nm was obtained from Sigma-Aldrich Ltd. The 15 nm nanoparticles showed higher dispersion than those obtained in the ILTSR PAS. The size of the particles was determined by Brunauer–Emmett–Teller method. The surface area of the powders were 533.6, 143.2 and 64.1 m^2/g for 5, 15 and 42 nm nanoparticles, respectively.

The powder of an amount of 0.15 g was placed inside the cell after the bottom cap was fixed to the glass tube. Then the upper cap was also glued and the assembled cell was installed in the cryostat. The nanopowder volume density in the cell was 7%. The cell prepared in the way described above was placed in the measuring chamber of the cryostat. At the beginning of the experiment the temperature of the cell was lowered to a little bit above the triple point temperature of argon and argon gas was let to the cell, whereupon the condensation to its liquid phase began. During the condensation the temperature of the upper part of the cell was kept a few Kelvins higher than the temperature of the bottom so that the liquid gradually filled the cell from its bottom to the top. In this way we obtained an argon–SiO_2 liquid nanocomposite. Finally, the temperature of the bottom of the ampoule was slowly lowered — the liquid solidified forming an argon–SiO_2 cryocrystal nanocomposite. Cooling rate during the crystal growth was 3 K/h. After crystallization the nanocomposite was cooled down to the temperature of the thermal conductivity measurement at the cooling rate of 6 K/h.

In the process of determination of the thermal conductivity two distorting factors were taken into account: 1. The parasitic temperature gradient being a result of the heat radiation due to the temperature mismatch of the LHe thermal shield of the measuring cell and the sample and 2. The heat transported by the cell glass wall. To determine the first one, the measurements of the parasitic temperature gradient was carried out at various temperatures for each of the samples. As for the second one, the measurement of the dependence of the thermal conductivity coefficient of empty cell was performed in a separate experiment.

The random error of the thermal conductivity measurement in low temperatures did not exceed 1.5%, whereas

above 20 K it increased to 3%, mostly due to effects connected with spurious heat leaks. The systematic error did not exceed 3%.

Results and discussion

Thermal conductivity $\kappa(T)$ of the investigated nanocomposites and pure solid argon [16] are both presented in Fig. 1. For all argon–SiO₂ cryocrystal nanocomposites their thermal conductivity is lower than that of the bulk polycrystal argon [16–20]. The dependence $\kappa(T)$ shows a behavior typical for polycrystaline atomic crystals. With decreasing temperature the thermal conductivity initially increases according to the relationship $\kappa(T) \propto T$ then it attains a maximum and finally decreases as T^2. The behavior of $\kappa(T) \propto T^2$ is specified by dominant scattering of phonons by static strain fields surrounding dislocations [19]. The thermal conductivity of Ar–15 nm SiO₂ nanocomposite shows the smallest thermal conductivity. In the temperatures below 6 K the dependence can be approximated by $\kappa(T) \propto T^n$, where $n = 1.55$. Here it should be noted that the exponent $n < 2$ is, in some cases, the manifestation of a complex fractal structure of a substance [21–23].

For the preliminary analysis of the temperature dependence of thermal conductivity coefficient of the investigated samples we used a simple thermal conductivity model. Assuming that the heat is conducted along parallel paths, the thermal conductivity coefficient of components of a medium is additive. It follows that the thermal conductivity of two-component medium consisting of polycrystalline argon and nano-SiO₂ material can be approximated as a weighted sum of the thermal conductivities of solid argon
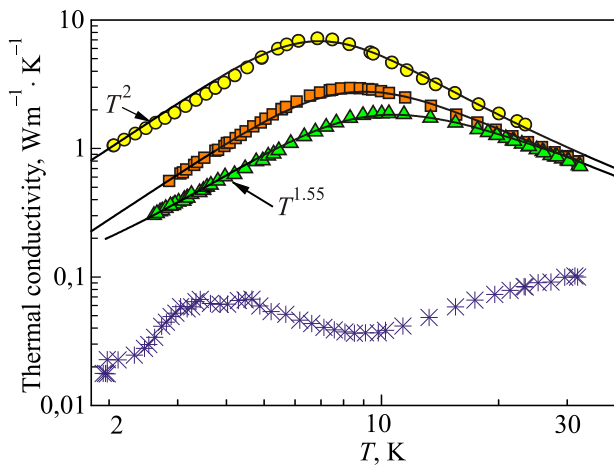
$\kappa_{Ar}(T)$ and the nanoparticles of SiO₂ $\kappa_{SiO_2}(T)$ according to the following expression [24]:

$$\kappa(T) = \kappa_{Ar}(T) + \kappa_{SiO_2}(T). \tag{1}$$

The value of thermal conductivity of the argon–SiO₂ nanocomposite consists of the thermal conductivity $\kappa_{Ar}(T)$ of solid argon which is a medium for SiO₂ particles. The thermal conductivity $\kappa_{Ar}(T)$ is determined by phonon transport of the heat [25–29]. The contribution of thermal conductivity coefficient of SiO₂ nanoparticle, $\kappa_{SiO_2}(T)$, to the sum $\kappa(T)$ is small — in Fig. 1 such low-thermal conductivity $\kappa_{SiO_2}(T)$ obtained for the SiO₂ nanopowder of 15 nm alone was depicted. The thermal conductivity $\kappa_{SiO_2}(T)$ shows a dependence which is almost not influenced by the size of SiO₂ nanoparticles in the interval from 5 up to 42 nm. In Fig. 1 the dependence $\kappa_{SiO_2}(T)$ for 15 nm nanopowder is shown. The data obtained for the nanoparticles of linear dimensions of 5 and 42 nm agree with the shown ones within the experiment accuracy.

Since the contribution of nanoparticles to the resultant thermal conductivity of the investigated nanocomposite is negligible, in further analysis we focus exclusively on argon matrix phonons. Let us take into account only two mechanisms of heat carrier scattering: phonon-phonon interactions in U-processes and scattering of phonons by dislocations. The influence of grain boundary scattering is small in the thermal conductivity of the current samples [25]. Therefore, the dependence $\kappa_{Ar}(T)$ can be written as a reciprocal of the sum of thermal resistance due to phonon dislocation scattering and phonon-phonon scattering in U-processes with the following expression

$$1/\kappa_{Ar}(T) = 1/\kappa_{dis}(T) + 1/\kappa_{ph}(T), \tag{2}$$

where $k_{ph}(T) = AT^{-1}e^{E/T}$ describes the three-phonon processes and $\kappa_{dis}(T) = BT^2$ is the contribution of dislocation scattering. We fitted equation (2) to all the data obtained in the described here experiment. The solid lines shown in Fig.1 are results of the fitting. As one can see from the figure, the fittings describe the experimental data well, both for pure argon and argon–SiO₂ nanocomposites. The best fit parameters *A, B* and *E* are given in Table 1.

Fig. 1. Thermal conductivity of: pure solid argon (●) [16], SiO₂ nanoparticles of 15 nm linear dimension (✳), argon with SiO₂ nanoparticles of linear dimentions 5 nm (■) and 15 nm (▲). For the clarity of the picture, the data obtained for solid argon–SiO₂ nanoparticles of linear dimension of 42 nm were not shown. Three solid lines are model approximation of temperature dependence of the thermal conductivity of the solid argon and the investigated nanocomposite samples.

Table 1. Value of the parameters *A, B* and *E* of equation (2), for which the experimentally obtained dependence of the thermal conductivity of the investigated nanocomposites is best approximated.

Sample	Three-phonon U-processes		Dislocation scattering
	A, Wm⁻¹	*E*, K	*B*, Wm⁻¹·K⁻³
Pure Ar	21	11.5	0.25
Ar–5 nm SiO₂	21	8	0.07
Ar–15 nm SiO₂	21	5	0.036
Ar–42 nm SiO₂	20	7	0.06

In the framework of the model described above, the reduction of the thermal conductivity of the investigated nanocomposite is a result of an increase, in comparison to the pure argon polycrystal, of intensity of phonon scattering by dislocations. This may be an effect of an increase of the dislocation density in the nanocomposite, which in turn may be a combined result of heterogeneous growth of polycrystalline argon with the nanoparticles being the crystallization centers and the cooling process of the composite in pre-melting temperature region, wherein solid argon shows a large value of the coefficient of linear expansion [30,31]

A deviation from the dependence $\kappa(T) \propto T^2$ for the sample of argon–15 nm SiO_2 at temperatures $T < 6$ K should be noted. The deviation may be a result of contribution of the thermal conductivity of nanopowder to the total thermal conductivity. It can be observed due to low thermal conductivity of the investigated sample.

Summary

The dependence of thermal conductivity coefficient on temperature of Ar–SiO_2 nanocomposites was experimentally investigated in the temperature range 2–35 K by steady-state heat flow method. The investigated samples consisted of solid argon with SiO_2 amorphous nanoparticles embedded in the argon crystalline matrix. The fraction of silica was 7% of the volume of the investigated samples. It was found that the thermal conductivity of the Ar–SiO_2 nanocomposites can be described by taking into account merely two argon crystal phonon scattering mechanism: phonon-phonon scattering in U-processes and scattering of phonons by the crystal dislocations.

1. M.T. Hung, C.C. Wang, J.C. Hsu, J.Y. Chiou, S.W. Lee, T.M. Hsu, and P.W. Li, *Appl. Phys. Lett.* **101**, 251913 (2012).

2. Y. Ma, R. Heijl, and A.E.C. Palmqvist, *J. Mater. Sci.* **48**, 2767 (2013).

3. Y. Ezzahri and K. Joulain, *J. Appl. Phys.* **113**, 043510 (2013).

4. M.L. Lee and R. Venkatasubramanian, *Appl. Phys. Lett.* **92**, 053112 (2008).

5. W. Kim and A. Majumdar, *J. Appl. Phys.* **99**, 084306 (2006).

6. R. Prasher, *J. Heat Transfer* **128**, 627 (2006).

7. N. Mingo, D. Hauser, N.P. Kobayashi, M. Plissonnier, and A. Shakouri, *Nano Lett.* **9**, 711 (2009).

8. W. Kim, S.L. Singer, A. Majumdar, J.M.O. Zide, D. Klenov, A.C. Gossard, and S. Stemmer, *Nano Lett.* **8**, 2097 (2008).

9. W. Kim, J. Zide, A. Gossard, D. Klenov, S. Stemmer, A. Shakouri, and A. Majumdar, *Phys. Rev. Lett.* **96**, 045901 (2006).

10. W. Kim, S.L. Singer, and A. Majumdar, *J. Phys. Conf. Ser.* **92**, 012085 (2007).

11. G.K. White and S.B. Woods, *Philos. Mag.* **3**, 785 (1958).

12. A. Berne, G. Boato, and M. De Paz, *Cimento B Series* **10**, 182 (1966).

13. F. Clayton and D.N. Batchelder, *J. Phys. C* **6**, 1213 (1973).

14. D.K. Christen and G.L. Pollack, *Phys. Rev. B* **12**, 3380 (1975).

15. R.V. Nikonkov, P. Stachowiak, T.V. Romanova, A. Jeżowski, and V.V. Sumarokov, *Fiz. Nizk. Temp.* **41**, 625 (2015) [*Low Temp. Phys.* **41**, 492 (2015)].

16. P. Stachowiak, V.V. Sumarokov, J. Mucha, and A. Jeżowski, *Phys. Rev. B* **58**, 2380 (1998).

17. I.N. Krupskii and V.G. Manzhelii, *Sov. Phys. JETP* **2**, 1097 (1969).

18. L. Finegold and N.E. Phillips, *Phys. Rev. B* **177**, 1383 (1969).

19. F. Clayton and D.N. Batchelder, *J. Phys. C: Solid State Phys.* **6**, 1213 (1973).

20. D.K. Christen and G.L. Pollack, *Phys. Rev. B* **12**, 3380 (1975).

21. D. Szewczyk, A. Jezowski, G.A. Vdovichenko, A.I. Krivchikov, F.J. Bermejo, J.L. Tamarit, andJ.W. Taylor, *J. Phys. Chem. B* **119**, 8468 (2015).

22. M. Hassaine, R.J. Jiménez-Riobóo, I.V. Sharapova, O.A. Korolyuk, A.I. Krivchikov, and M.A. Ramos, *J. Chem. Phys.* **131**, 174508 (2009).

23. A.I. Krivchikov, O.A. Korolyuk, and I.V. Sharapova, *Fiz. Nizk. Temp.* **38**, 95 (2012) [*Low Temp. Phys.* **38**, 74 (2012)].

24. A.I. Krivchikov, B.Y. Gorodilov, O.A. Korolyuk, V.G. Manzhelii, O.O. Romantsova, H. Conrad, and D.D. Klug, *Phys. Rev. B* **73**, 064203 (2006).

25. S. Ju and X. Liang, *J. Appl. Phys.* **108**, 104307 (2010).

26. J.E. Turney, E.S. Landry, A.J.H. McGaughey, and C.H. Amon, *Phys. Rev. B* **79**, 064301 (2009).

27. H. Kaburaki, J. Li, S. Yip, and H. Kimizuka, *J. Appl. Phys.* **102**, 043514 (2007).

28. Z. Zhong and X. Wang, *J. Appl. Phys.* **100**, 044310 (2006); P. Heino, *Phys. Rev. B* **71**, 144302 (2005).

29. K.V. Tretiakov and S. Scandolo, *J. Chem. Phys.* **121**, 11177 (2004).

30. O.G. Peterson, D.N. Batchelder, and R.O. Simmons, *Phys. Rev. B* **150**, 703 (1966).

31. C.R. Tilford and C.A. Swenson, *Phys. Rev. B* **5**, 719 (1972).